Journal of Zhejiang University-SCIENCE A (Applied Physics & Engineering) 2023 24(9):801-816
www.jzus.zju.edu.cn; www.springer.com/journal/11582
E-mail: jzus_a@zju.edu.cn

Research Article

https://doi.org/10.1631/jzus.A2200516

A data-driven approach for modeling and predicting the thrust force of a tunnel boring machine

Lintao WANG[1], Fengzhang ZHU[1], Jie LI[1,2]✉, Wei SUN[1]

[1]*School of Mechanical Engineering, Dalian University of Technology, Dalian 116024, China*
[2]*North Automatic Control Technology Institute, Taiyuan 030006, China*

Abstract: Thrust prediction of a tunnel boring machine (TBM) is crucial for the life span of disc cutters, cost forecasting, and its design optimization. Many factors affect the thrust of a TBM. The rock pressure on the shield, advance speed, and cutter water pressure will all have a certain impact. In addition, geological conditions and other random factors will also influence the thrust and greatly increase the difficulty of modeling it, seriously affecting the efficiency of tunnel excavation. To overcome these challenges, this paper establishes a thrust prediction model for the TBM based on the combination of on-site quality record data and surrogate model technology. Firstly, the thrust composition and influencing factors are analyzed and the thrust is modeled using a surrogate model based on field data. After main factor screening based on the Morris method, the accuracy of the surrogate model is greatly improved. The Kriging model with the highest accuracy is selected to model the thrust and predict the thrust of the unexcavated section. The results show that the thrust model has better thrust prediction by selecting similar conditions for modeling and reasonably increasing modeling samples. The thrust prediction method of TBM based on the combination of field data and surrogate model can accurately predict the dynamic thrust of the load and can also accurately estimate its statistical characteristics and effectively improve the excavation plan.

Key words: Tunnel boring machine (TBM); Thrust prediction; Surrogate model; Morris method

1 Introduction

A tunnel boring machine (TBM) is a large machine widely applied in tunnel construction, especially in hard rocks. During the tunnel boring process, the TBM needs to overcome the resistance in its axial direction to thrust forward. Generally, the total resistance in the axial direction of the TBM is termed the thrust force, which can reach as high as 23060 kN for a Φ8 m TBM. As a key tunneling parameter, the thrust force can directly influence the life span of disc cutters, the forecast cost, and the selection of the TBM. Therefore, for the design or control of the TBM, it is very important to predict the thrust according to the specific geological conditions. However, the estimation and accurate prediction of thrust are quite challenging. On the one hand, the thrust is related to many factors, such as forward speed, cutterhead speed, and rock hardness. However, in the process of thrust modeling and prediction of the TBM, there is no clear corresponding relationship between the above factors and thrust. On the other hand, in the process of tunneling, the thrust is essentially a random variable due to many uncertainties in the geological conditions and the rock stripping process. Because of these uncertainties, the difficulties of thrust force prediction for a TBM are increased and many existing thrust force models cannot be applied directly. In addition, the failure to accurately predict the thrust of TBM will seriously affect the excavation plan and efficiency of the tunnel and is not conducive to improving the excavation planning and maximizing the advance rate.

In the past decades, scholars at home and abroad have done much research on thrust prediction in shield machines (Lv et al., 2022). Shield machines of the earth pressure balance type (EPB-type), which are intended for soil or soft rock, were invented and investigated earlier than the TBM. For the thrust force

✉ Jie LI, leejiedlut@163.com
Jie LI, https://orcid.org/0000-0002-5263-1651

Received Oct. 28, 2022; Revision accepted Feb. 26, 2023;
Crosschecked Aug. 2, 2023

(F) prediction of the EPB-type shield machine, Krause (1976) proposed an empirical formula $F=\beta D^2$ (D is the diameter of the tunneling machine, and β is the empirical coefficient) by statistical analysis of engineering data from hundreds of shield tunneling machines. Due to its simplicity, the Krause empirical model can be used for preliminary load estimations. However, the estimated load based on the above methods is often very high and the range of values is too wide (Zhang Q et al., 2014). To reduce the impact of uncertainty in the empirical model of accurate thrust prediction, researchers have tried to establish an analysis model based on the analysis of the interaction mechanism between shield machine and soil. For example, Shi et al. (2011) put forward an analysis model of shield machine thrust of an EPB-type by comprehensively considering the structural parameters and geological conditions. Copur et al. (2014) investigated the stochastic characteristics of an EPB-type shield machine excavation by implementing a stochastic model in a deterministic model. Zhang Q et al. (2013) put forward a theoretical model of load prediction for an EPB-type under the working condition of soil–rock interlaced ground. In that model, the thrust is calculated by separately calculating the thrust components, and then combining them to obtain the total thrust. These models have been experimentally proved to be quite precise for thrust force estimation and prediction in soft soil.

For the load analysis of TBM in hard rock, the existing research is mainly focused on the thrust load on the disc cutter. At present, tool load models for flat and wedge tools have been developed (Li et al., 2011). In addition, a prediction model of the cutting force of the disc cutter has been developed; it is generally called the model for cutting force estimation of disc cutters (CSM) (Hassanpour et al., 2010). Barton (1999) put forward a model for predicting TBM performance by Q(TBM) methods (Q means the rock mass quality). Zhang ZH et al. (2014) proposed a new method to predict the life and abrasion of a disc cutting machine and the time for its replacement. In addition, the field penetration index (FPI) has provided a new way of predicting TBM performance (Yagiz, 2017). The relationship between the force acting on the tool and the rock properties can be obtained by using the above model. Based on the above analysis, similarly, according to the thrust prediction method of the EPB-type shield machine, the thrust prediction model and the load of the cutter of the TBM can be obtained. However, the rock cutting principle of the TBM is totally different from that of an EPB-type shield machine. The scraper of the EPB-type shield machine cuts off the soil continuously during the working process, that is, all scrapers on the cutterhead are always in contact with the soil. By contrast, the disc cutter is in discontinuous contact with the rock during the operation of the TBM. At any given moment, it is difficult to obtain the position and quantity of cutter contacting with the rock in a TBM. Hence, the thrust force of the TBM, random in nature, cannot be obtained directly via summing the load on each cutter as can be done for the EPB-type. In addition, the uncertainty of factors such as cutterhead and geological conditions also increases the difficulty of accurate prediction of the thrust. Therefore, it is necessary to develop a model that can accurately predict the TBM thrust.

Nowadays, machine learning (ML), especially deep learning (DL), has received extensive attention due to its successful application to solving complex engineering and mathematical problems (Iliadis et al., 2022). Rosso et al. (2023) proposed an automatic classification framework for highway tunnel issues based on convolutional neural network (CNN), which improved the efficiency of indirect measurement methods. Lin et al. (2022) proposed a hybrid model of particle swarm optimization (PSO) and long short-term memory (LSTM) neural network. Based on the above, a framework for automatic data collection and model application during tunnel excavation is developed. By collecting tunnel construction data for training and testing, the results show that the model has the best performance and can be used to process the measured data of the shield machine automatic monitoring system. By studying the coupling dynamic characteristics of the cutterhead system of TBM under multi-source uncertainty, Huo et al. (2022) established a geological uncertainty coupling model and a disc cutter uncertainty coupling model. By combining the above model with the load interval boundary, a multi-source uncertainty dynamic model of TBM was established. The results show that the dynamic model considering multi-source uncertainty can provide theoretical guidance for the design of the cutting head damping structure. In addition, recent research work has begun to incorporate prior information and uncertainties, thereby improving the generalization ability of data-driven models. Data-driven generalization ability can be

significantly improved by using Bayesian neural network (BNN) (Yang et al., 2021), physical information neural network (Raissi et al., 2019), and multi-fidelity BNN (Meng et al., 2021). The above model has been widely used in solving practical engineering problems such as function approximation and solving inverse problems based on partial differential equations. Hence, ML tools provide a new way to model the TBM and predict thrust under complex conditions.

In view of the shortcomings of the above research in thrust modeling and prediction of TBM and the successful application of ML tools in complex tunnel engineering problems, this paper proposes a data-driven thrust preliminary modeling and prediction method based on probability theory. The rest of the paper is organized as follows. In Section 2, the composition of thrust of TBM is introduced and the sample data are preprocessed. By analyzing the source of the TBM thrust, the influencing factors of thrust are established. In Section 3, the surrogate model of thrust of the TBM based on different kernel functions is established based on tunnel construction data, and the accuracy of different surrogate models is compared. After screening the main influencing factors based on the Morris algorithm, the accuracy of the surrogate model is greatly improved. In Section 4, based on different excavated parts, three Kriging (KRG) models are established to predict the thrust of the unexcavated part, and are compared with the recorded site data to obtain the overall fluctuation of the prediction accuracy of the thrust agency model. The accuracy of the three thrust prediction models is discussed based on the relative error, and an algorithm for further improving the thrust prediction model is proposed. In Section 5, based on the difference between the predicted value and the actual value of thrust in different prediction models, the generalization ability of the KRG model and the subsequent improvement methods are discussed in combination with the thrust modeling process. Finally, conclusions are provided in Section 6.

2 Compositions and influential factors of thrust force

The TBM is mainly composed of a cutterhead, a main bearing, a thrust system, and a gripper mechanism. The gripper system is used during the driving process of the TBM, and acts on the side wall of the tunnel to advance it. The cutterhead of the TBM can be continuously turned and the gripper shoes are pushed on the side wall to push the machine forward in reaction. At the end of one stroke of the TBM, the rear legs of the machine are lowered, and the grippers and propulsion cylinders are retracted. When the propel cylinder retracts, the gripper assembly is repositioned for the next boring cycle. At the beginning of the next boring cycle, the gripper extends and the rear legs are raised. TBM can operate continuously according to the above process. It can be seen from the above that the tunneling process of TBM is a discontinuous periodic tunneling process.

This study takes the tunnel project in a central city of a province in China as an example. The total length of the main line of the project is 69.855 km, and the construction area is mainly valleys and hills. The above geological areas are classified according to the types of surrounding rock. Type III surrounding rock is the main surrounding rock, accounting for more than 50%. Type IV surrounding rock is a common surrounding rock, accounting for 24.9%. The excavation section is circular, and the main technical parameters of TBM are shown in Table 1.

Table 1 Major technical specifications of the Φ7.93 m TBM

Parameter	Value
Excavation diameter (m)	7.93
Length of machine (m)	22
Host length (m)	300
Number of hobs	47
Number of propulsion cylinders	4
Cylinder stroke (mm)	1900
Maximum working pressure (MPa)	35
Maximum total propulsion (kN)	23060

During the excavation process, the parameters and data related to the excavation load are recorded by sensors. The data measured and sampled on site include a large quantity of records and many parameter variables, but some of them are not very relevant to the tunneling load. Therefore, to improve efficiency and speed up the process of TBM thrust modeling, it is necessary to process the data and analyze the source of thrust. Considering the propulsion characteristics of TBM, data preprocessing is first performed. Data preprocessing can divide the excavation cycle

and remove the non-working state data. In the process of TBM tunneling, the thrust force F, cutterhead advance speed v_s, cutterhead torque T, and cutterhead rotation speed v_c are not zero. Therefore, a binary state discriminant function K can be established based on the above indicators and used as the basis for data preprocessing.

$$K=f(F)\,f(T)\,f(v_s)\,f(v_c),$$
$$K=\begin{cases}1, & \text{working condition,}\\ 0, & \text{off position.}\end{cases} \tag{1}$$

The thrust force of the TBM consists of three main parts, i.e., the normal force between the cutterhead and the rock F_1, the frictional force on the shield F_2, and the traction force of the backup device F_3. The schematic description of the thrust force is shown in Fig. 1. During the tunnel excavating process, the thrust force is directly influenced by the operating and geological parameters (Zheng et al., 2016). For example, the rock pressure on the shield under different geological conditions will affect the friction force.

Moreover, the normal force acting on the cutterhead will increase with an increase in the tunneling speed of the TBM. In addition, during the propulsion of the TBM, its operating attitude will affect the rock pressure on the shield and thus have a certain impact on the thrust. As shown in Table 2, through factor

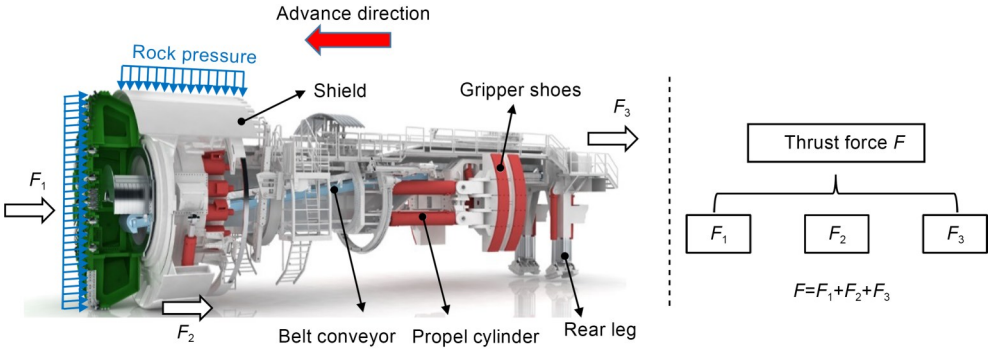

Fig. 1 Composition analysis of the thrust force

Table 2 Influential factors of the thrust force

No.	Factor	Notation	Value	
			Lower bound	Upper bound
1	Front shield pitch angle (°)	α_a	0.3974	0.5270
2	Front shield roll angle (°)	α_b	−0.2254	0.1439
3	Left shield pressure (MPa)	p_l	3.2763	6.7216
4	Right shield pressure (MPa)	p_r	1.1685	3.2913
5	Top shield pressure (MPa)	p_t	4.2119	4.3001
6	Left rear support pressure (MPa)	p_{lr}	0.2170	0.5899
7	Right rear support pressure (MPa)	p_{rr}	1.4202	1.6107
8	Pressure gripper shoes (MPa)	p_g	32.8140	33.7184
9	Cutter water pressure (MPa)	p_c	0.5749	0.7243
10	Inner seal pressure (MPa)	p_i	0.0344	0.0677
11	Outer seal pressure (MPa)	p_o	0.0415	0.0525
12	Cutterhead rotation speed (r/min)	v_c	57.026	64.638
13	Penetration (mm/r)	λ	46.192	114.247
14	Cutterhead advance speed (mm/min)	v_s	263.935	685.668
15	Left gripper shoes pitch angle (°)	β_a	−2.7207	−2.5299
16	Left gripper shoes roll angle (°)	η_a	−3.0081	−2.9680
17	Right gripper shoes pitch angle (°)	β_b	−1.3655	−1.1552
18	Right gripper shoes roll angle (°)	η_b	1.8651	1.9401
19	Host belt speed (mm/s)	v_h	3.1944	3.3212
20	Bridge belt conveyor speed (mm/s)	v_b	2.6732	2.6768
21	Turn the belt conveyor speed (mm/s)	v_t	2.7539	2.7575

analysis on the source of thrust, 21 variables that may affect the thrust are selected.

3 Thrust force modeling based on surrogate models

3.1 Selecting the appropriate surrogate models

The aim of data-driven thrust force modeling is to describe the relationship between the thrust force and its influential parameters mathematically, based on the hidden information in the on-site construction data. Therefore, the key point of this work is to find a model $\hat{y}=\hat{y}(\boldsymbol{x})$ by exploring the on-site data which will represent the true relationship between thrust force and its influential parameters $\boldsymbol{x}$, where $\boldsymbol{x}$ is the input vector that constitutes the thrust model of the TBM listed in Table 3.

Based on the analysis in Section 2, it is difficult to establish a theoretical model of thrust of the TBM because of the many factors affecting the thrust and the uncertainty of the geological conditions. Approximation models are methods to approximate a group of input variables (independent variables) and output variables (response variables) through mathematical models. Such a model can establish empirical formula through training samples to obtain a quantitative relationship between input and output variables. Thus, the surrogate model provides an effective alternative method for establishing the relationship between thrust and its influencing parameters from the TBM. Surrogate modeling can bridge the gaps between the results of a limited number of inputs and capture the major properties of an expensive experiment or numerical simulation. For the ith observation point $\boldsymbol{x}^{(i)}=(x_1^{(i)}, x_2^{(i)}, \cdots, x_{n_{\mathrm{dv}}}^{(i)})$ of a n_{dv}-variable design space, $y^{(i)}$ represents the positive real part of the eigenvalue of the model. In this work, the key of surrogate model modeling is the selection of an appropriate surrogate model. Firstly, an appropriate surrogate model is determined by comparing the accuracy of different surrogate models, and then the parameters in the surrogate model are determined by training the surrogate model samples with field data. After the parameters are determined, they can be used to predict the subsequent thrust. As it is not clear which surrogate models are more accurate in thrust force modeling, four commonly used surrogate models, namely, cubic polynomial response surface method (PRS) (Myers et al., 2016), KRG model (Sacks et al., 1989), support vector regression (SVR) (Williamson et al., 2001), and radial basis function (RBF) (Buhmann, 2000; Gutmann, 2001; Regis and Shoemaker, 2005; Yuan et al., 2010) are considered and shown in Table 3.

In Table 3, m_1 is the order of polynomials. In the PRS model, x_i is the ith component of the n_{dv}-dimensional predicted value. b_0, b_i, b_{ij}, and b_{ijk} are regression constants and are obtained by the least square method. In the RBF model, $\varphi\left(\| \boldsymbol{x}-c^{(i)} \|\right)$ is an RBF used to estimate the distance between the input point and the center point. n_{c} is the number of basis functions. $c^{(i)}$ denotes the ith of the n_{c} basis function centers. λ_i is the weight coefficient. σ_1 is the normal number parameter of the multiple quadric surface, whose value is greater than 0. In addition, it is a shape parameter. Here we take $\sigma_1=1$. In SVR model, $w_1^{(i)}$ is the weight coefficient. $k(\boldsymbol{x}, \boldsymbol{x}^{(i)})$ is a Gaussian kernel function. n is the number of samples. σ_2 is a hyperparameter, and the hyperparameter value is $\sigma_2=2$. In addition, b is a constant. The KRG model consists of linear regression and a Gaussian random process. $R(\boldsymbol{x}^{(i)}, \boldsymbol{x}^{(j)})$ is a Gaussian correlation function. θ_k is the kth relevant parameter of the fitting model. $x_k^{(i)}$ and $x_k^{(j)}$ are the kth dimension values of $\boldsymbol{x}^{(i)}$ and $\boldsymbol{x}^{(j)}$, respectively.

Table 3 Parameters and functions of four commonly used surrogate models

Surrogate model	Approximate function $\hat{y}(\boldsymbol{x})$	Correlation function (radial basic, kernel)
PRS	$b_0+\sum_{i=1}^{m_1} b_i x_i+\sum_{i=1}^{m_1}\sum_{j=1}^{m_1} b_{ij} x_i x_j+\sum_{i=1}^{m_1}\sum_{j=1}^{m_1}\sum_{k=1}^{m_1} b_{ijk} x_i x_j x_k$	No
RBF	$\sum_{i=1}^{n_c} \lambda_i \varphi\left(\| \boldsymbol{x}-c^{(i)} \|\right)$	$\varphi\left(\| \boldsymbol{x}-c^{(i)} \|\right)=\sqrt{\| \boldsymbol{x}-c^{(i)} \|^2+\sigma_1^2}$
SVR	$\sum_{i=1}^{n} w_1^{(i)} k(\boldsymbol{x}, \boldsymbol{x}^{(i)})+b$	$k(\boldsymbol{x}, \boldsymbol{x}^{(i)})=\exp\left(\frac{\| \boldsymbol{x}-\boldsymbol{x}^{(i)} \|^2}{2\sigma_2^2}\right)$, $\sigma_2=2.0$
KRG	$\hat{\beta}+\boldsymbol{r}^{\mathrm{T}}(\boldsymbol{x})\boldsymbol{R}^{-1}(\boldsymbol{y}-\boldsymbol{f}\hat{\beta})$	$R(\boldsymbol{x}^{(i)}, \boldsymbol{x}^{(j)})=\exp\left(-\sum_{k=1}^{n_{\mathrm{dv}}} \theta_k \| x_k^{(i)}-x_k^{(j)} \|^2\right)$, $0.05\leqslant\theta_k\leqslant 100$

n_{dv} is the dimension of $\boldsymbol{x}$. $\hat{\beta}$ is the estimated value of the regression coefficient vector. $\boldsymbol{r}^{\mathrm{T}}(\boldsymbol{x})$ is the correlation matrix between the sample point and the unknown point. $\boldsymbol{y}$ is the sample response column vector. $\boldsymbol{f}$ is a unit column vector. $\boldsymbol{R}$ is an n-dimensional symmetric matrix composed of $R(\boldsymbol{x}^{(i)}, \boldsymbol{x}^{(j)})$.

It can be seen from the second section that by analyzing the thrust source of the TBM, we have identified 21 key design variables and obtained the sample data set from the data recorded by sensors in the tunnel. Therefore, the modeling of the following surrogate model enters the parameter estimation and training stage. Here, we use the maximum likelihood estimation and cross-validation method to minimize the loss function (Sun et al., 2020).

3.1.1 Maximum likelihood estimation

Given a set of parameters $\boldsymbol{w}$ and model $\hat{f}(\boldsymbol{x}, \boldsymbol{w})$, we can calculate the probability of the number set $\{(\boldsymbol{x}^{(1)}, y^{(1)}\pm\boldsymbol{\varepsilon}), (\boldsymbol{x}^{(2)}, y^{(2)}\pm\boldsymbol{\varepsilon}), \cdots, (\boldsymbol{x}^{(n)}, y^{(n)}\pm\boldsymbol{\varepsilon})\}$ generated by $\hat{f}$. $\boldsymbol{\varepsilon}$ is very small, which is a constant margin around each point. When the random distribution of error $\boldsymbol{\varepsilon}$ satisfies the normal distribution with standard deviation σ, the probability of the data set is:

$$P=\frac{1}{(2\pi\sigma^2)^{n/2}}\prod_{i=1}^{n}\left\{\exp\left[-\frac{1}{2}\left(\frac{y^{(i)}-\hat{f}(\boldsymbol{x},\ \boldsymbol{w})}{\sigma}\right)^2\right]\boldsymbol{\varepsilon}\right\}. \quad (2)$$

To simplify the calculation, the natural logarithm is negative and minimized:

$$\min_{\boldsymbol{w}}\sum_{i=1}^{n}\frac{\left[y^{(i)}-\hat{f}(\boldsymbol{x},\ \boldsymbol{w})\right]^2}{2\sigma^2}-n\ln\boldsymbol{\varepsilon}. \quad (3)$$

When we assume a constant σ and $\boldsymbol{\varepsilon}$, it can be simplified to the famous least squares criterion:

$$\min_{\boldsymbol{w}}\sum_{i=1}^{n}\left[y^{(i)}-\hat{f}(\boldsymbol{x},\ \boldsymbol{w})\right]^2. \quad (4)$$

3.1.2 Cross-validation

Cross-validation is to divide the data (randomly) into q identical subsets, and then remove one of the subsets in turn and fit the model with the remaining $q-1$ subsets. Then, the loss function is calculated to measure the error between the predicted value and the actual value of the subset removed by each iteration. Finally, in the q iteration processes, the contribution value of the loss function L is accumulated. In fact, when fewer subsets are used, additional benefits are often obtained. The computational cost of cross-validation is reduced by reducing the number of models that must be fitted. In this study, the data set is divided into two parts, 80% of the data is the training set, and 20% of the data is the test set.

3.1.3 Loss function

This study determines the loss function according to the strategy of empirical risk minimization. To minimize the error between the benchmark and the prediction, when the loss function is lower than a specific tolerance ε_0, the training process can be considered to converge and stop (Masi et al., 2021). The calculation formula of the loss function is as follows:

$$L(\boldsymbol{w})=\frac{1}{2}\sum_{i=1}^{n}\left[y^{(i)}-\hat{f}(\boldsymbol{x},\ \boldsymbol{w})\right]^2. \quad (5)$$

In the process of surrogate model fitting, overfitting often occurs when the model is too flexible to some extent; the model often fits the data too finely within a certain range. Therefore, in addition to the model itself to be fitted, the noise is also fitted. Therefore, to prevent over-fitting, this study selects the model in the process of cross-validation, so as to select the optimal model.

To evaluate the modeling accuracy of the above four surrogate models, the correlation coefficient is introduced as the evaluation standard of each surrogate model. The correlation coefficient R^2 can be described as (Mullur and Messac, 2006; Tao et al., 2010):

$$R^2=1-\frac{\sum_{i=1}^{m}\left(y^{(i)}-\hat{y}^{(i)}\right)^2}{\sum_{i=1}^{m}\left(y^{(i)}-\bar{y}^{(i)}\right)^2}, \quad (6)$$

where m is the number of detection points; $y^{(i)}$ is the response of the detection point; $\hat{y}^{(i)}$ is the calculation result of the surrogate model; $\bar{y}^{(i)}$ is the average value of the response of the detection point. Additional sampling points are generated to check the error of the constructed surrogate model, where the square-error

is used as an error analysis indicator. According to Eq. (6), the nearer the R^2 value of surrogate model approximates to 1, the better its fitting capacity is. As shown in Fig. 2, the precision of the proxy model between thrust and input variables based on different kernel functions is different. Based on the R^2 values of the four models, it can be seen that the RBF model has the highest accuracy ($R^2=0.81$). However, the accuracy of the above four surrogate models cannot be used for accurate prediction of TBM thrust, compared with the accuracy of proxy models that can reach more than 0.9 in general. Here, the RBF model is selected as the model for qualitative analysis of the parameters in Section 3.2.

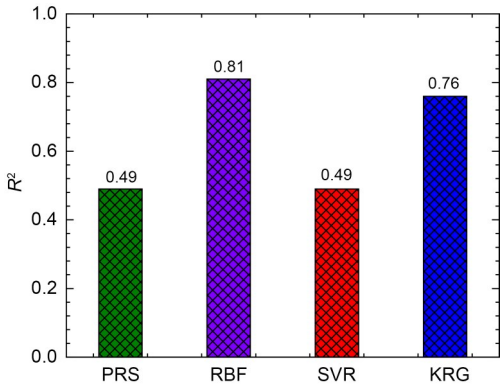

Fig. 2 Accuracy comparison of the four different surrogate models

3.2 Screening out main factors with sensitivity analysis

It can be seen from the above analysis that the accuracy of the surrogate model of the trained samples is not high, so it is necessary to screen factors to improve its accuracy. Among all the influencing factors of thrust, some are primary and some are secondary. To further improve the accuracy of the thrust force model, minor parameters that have little impact on the thrust force should be disregarded in thrust force modeling. According to Section 2, there are 21 independent variables in the thrust modeling. If all variables are taken into account, it is not conducive to the improvement of the accuracy of the surrogate model. Therefore, it is necessary to conduct sensitivity analysis and screen out the variables with greater impact (main factors). The Morris method is used here for sensitivity analysis. The Morris method is a discrete search method based on parameter space, which can study the model in a global range. The entire design space of the n_{dv}-dimensional input $\boldsymbol{x}$ is divided into p levels, so the value of the ith input x_i satisfies:

$$\begin{aligned}&\boldsymbol{x}=[x_1,\ x_2,\ \cdots,\ x_{n_{\mathrm{dv}}}]^{\mathrm{T}},\\&x_i\in\left\{0,\ \frac{1}{p-1},\ \frac{2}{p-1},\ \cdots,\ \frac{p-2}{p-1},\ 1\right\}.\end{aligned}\tag{7}$$

After an initial input $\boldsymbol{x}$ is given, the influence of the ith input on the output is called the ith fundamental effect, expressed as $d_i(\boldsymbol{x})$, which is calculated as:

$$\begin{aligned}&d_i(\boldsymbol{x})=\frac{(p-1)\times y}{\xi},\\&y=y\left(x_1,\ x_2,\ \cdots,\ x_{i-1},\ x_{i+\frac{\xi}{p-1}},\ x_{i+1},\ \cdots,\ x_{n_{\mathrm{dv}}}\right)-y(\boldsymbol{x}),\end{aligned}\tag{8}$$

where ξ is a preset amount of variation. To study the influence of multiple inputs on thrust, the Morris method needs to sample $(n_{\mathrm{dv}}+1)\times r_1$ times in total, where r_1 is the number of basic effects and can be obtained for any ith input. Herein, estimated means and standard deviations of elementary effect distributions are employed to distinguish the main influencing factors from the secondary factors. Based on the Morris algorithm (Morris, 1991), when the estimated means and standard deviations are far away from the zero point, then it can be explained that the input parameters have a great influence on the objective function. The estimated mean s_{m} and standard deviation s_{sd} of each influential parameter can be obtained as:

$$s_{\mathrm{m}}(\boldsymbol{x})=\frac{1}{n}\sum_{j=1}^{n}d_i^{(j)}(\boldsymbol{x}),\tag{9}$$

$$s_{\mathrm{sd}}(\boldsymbol{x})=\sqrt{\frac{1}{n}\sum_{j=1}^{n}\left(d_i^{(j)}(\boldsymbol{x})-s_{\mathrm{m}}(\boldsymbol{x})\right)^2},\tag{10}$$

where $d_i^{(j)}(\boldsymbol{x})$ is the ith basic effect of group j trials. When using the Morris method for sensitivity analysis, the specific values of parameters p, r_1, and ξ need to be reasonably determined. When selecting the specific values of p and ξ, it is recommended to use p as an even number and the parameter ξ satisfies $\xi=p/[2(p-1)]$. In addition, the selection of parameter r_1 is also closely related to the selection of parameter p. In summary, r_1=10 and p=4 is recommended here (Saltelli et al., 2004).

To evaluate the elementary effect distributions of variables, the RBF model is used in analysis of the parameters, and the equation of the RBF model (Breiman, 2001) is:

$$y(\boldsymbol{x})=\sum_{i=1}^{n}\lambda_i\sqrt{\|\boldsymbol{x}-c^{(i)}\|^2+\sigma_1^2}\,. \tag{11}$$

Using the Morris algorithm, the elementary effect distributions can be obtained according to Eqs. (9) and (10). Fig. 3 shows the main influential parameters. As shown in Fig. 3, among the estimated means and the standard deviations of elementary effects, the parameters away from the zero line of the means are the left shield pressure (p_l), the right shield pressure (p_r), the pressure gripper shoes (p_g), the penetration (λ), and the cutterhead advance speed (v_s). These five parameters have a large influence on the process of TBM excavation in the process of large influence. Among the five main influence parameters, the cutterhead advance speed v_s has the greatest influence on the thrust and is very important for the excavation plan of the TBM. In addition to the above five main factors, the estimated standard deviations s_{sd} and mean values s_m of the remaining 16 independent design variables are close to zero, so the impact of these 16 design variables on thrust is very small, and their impact can be ignored when building the surrogate model.

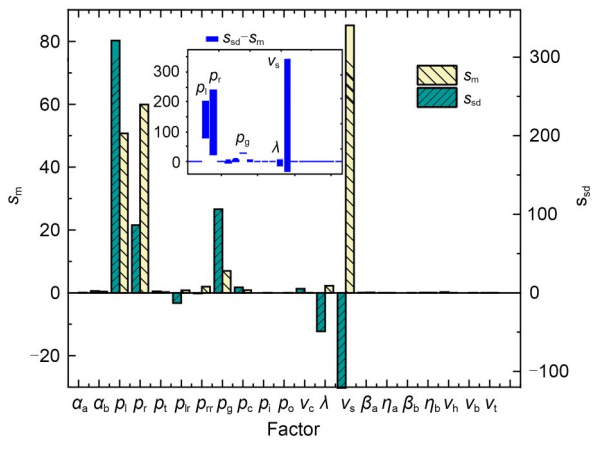

Fig. 3 Estimated means and standard deviations of elementary effect distributions

3.3 Constructing surrogate models with high accuracy

In this section, based on the main influential parameters, the TBM thrust force models are built. The number of samples selected is 200 and the number of the test samples is 50. The comparison of R^2 for the four surrogate models is shown in Fig. 4.

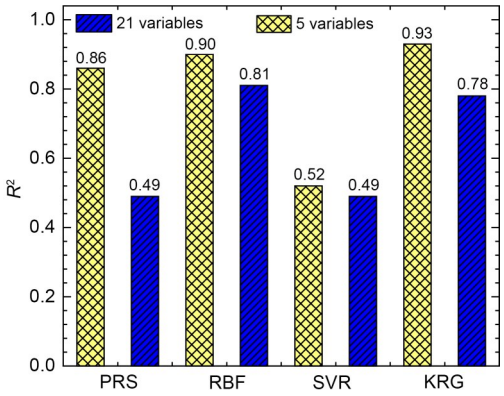

Fig. 4 Accuracy comparison of the main influential parameters for surrogate models

As shown in Fig. 4, when using the five main influence parameters to establish the surrogate model, the accuracy of the surrogate models has been effectively improved. In particular, the precisions of KRG and RBF models are greater than 0.9 after using the main factor modeling. In addition, compared with other surrogate models, the agency accuracy of the KRG model has reached the highest accuracy among the four agency models after being filtered by the main factors. It can be seen that the accuracy of the KRG model increases from $R^2=0.76$ to $R^2=0.93$. Therefore, when beginning to model the TBM thrust, the main influence parameters on the thrust force are identified and the parameters with less influence are removed thus reducing the dimensionality of the design variables and improving the accuracy of the model. After screening the main factors with the Morris method, this study uses the KRG model to model the thrust model of the TBM.

In addition, to avoid overfitting, this study takes the training set as the sample and the correlation coefficient R^2 as the evaluation index. The seven-fold cross-validation of the KRG model was performed to obtain the correlation coefficient of the TBM thrust model (Jean et al., 2022). The results are shown in Table 4. The results showed that the correlation coefficient R^2 was greater than 0.9. This shows that the established KRG model has a high predictive ability for TBM thrust.

In general, feature selection is the step before model development. However, based on the above

Table 4 Seven-fold cross-validation results

Data set number	R^2
1	0.97997
2	0.98102
3	0.98988
4	0.98080
5	0.97993
6	0.99799
7	0.97980

thrust surrogate model modeling process of TBM, this study first constructs the results of the thrust surrogate model and then performs feature selection. This is because this study first analyzes the source of TBM thrust and obtains 21 possible influencing factors, that is, the influencing factors are uncertain. The above influencing factors are used as model features and a surrogate model is constructed. The results show that the accuracy and prediction credibility of the surrogate model constructed by 21 design variables are low. Therefore, there are redundant features in the influencing factors of TBM thrust, so the Morris method is used for feature selection to further improve the accuracy of the model. The advantage of this is that all possible influencing factors in the TBM thrust modeling process are fully considered, and the subsequent feature selection further improves the prediction accuracy of the TBM.

As above mentioned, the KRG model is selected as the model of thrust and can be calculated using Eqs. (12)–(17).

$$F(\boldsymbol{x})=f(\boldsymbol{x})+Z(\boldsymbol{x}), \tag{12}$$

$$\mathrm{Cov}\left[Z(\boldsymbol{x}^{(i)}),\ Z(\boldsymbol{x}^{(j)})\right]=\sigma^2 R(\boldsymbol{x}^{(i)},\ \boldsymbol{x}^{(j)}). \tag{13}$$

In Eqs. (12) and (13), $F(\boldsymbol{x})$ is the unknown function; $f(\boldsymbol{x})$ is a known function of $\boldsymbol{x}$ (similar to the polynomial function in the response model, which provides a global trend of the design space); $Z(\boldsymbol{x})$ represents the stochastic process with a zero mean and a nonzero variance σ^2 as well as a nonzero covariance to model local deviations.

$$\hat{F}(\boldsymbol{x})=\hat{\beta}+\boldsymbol{r}^{\mathrm{T}}(\boldsymbol{x})\boldsymbol{R}^{-1}\left(\boldsymbol{y}-\boldsymbol{f}\hat{\beta}\right), \tag{14}$$

$$\boldsymbol{r}^{\mathrm{T}}(\boldsymbol{x})=\left[R(\boldsymbol{x},\ \boldsymbol{x}^{(1)}),\ R(\boldsymbol{x},\ \boldsymbol{x}^{(2)}),\ \cdots,\ R(\boldsymbol{x},\ \boldsymbol{x}^{(n)})\right]^{\mathrm{T}}, \tag{15}$$

$$\hat{\beta}=(\boldsymbol{f}^{\mathrm{T}}\boldsymbol{R}^{-1}\boldsymbol{f})^{-1}\boldsymbol{f}\boldsymbol{R}^{-1}\boldsymbol{y}, \tag{16}$$

$$R(\boldsymbol{x}^{(i)},\ \boldsymbol{x}^{(j)})=\exp\left(-\sum_{k=1}^{n_{\mathrm{dv}}}\theta_k\left|x_k^{(i)}-x_k^{(j)}\right|^2\right), \tag{17}$$

where $\boldsymbol{y}$ is the column vector with the length n containing the response sample value; $\boldsymbol{f}$ is a column vector of length n; n_{dv} is the number of design variables; $\theta_k\,(k=1,\ 2,\ \cdots,\ n_{\mathrm{dv}})$ are the unknown correlation parameters used to fit the model; $|x_k^{(i)}-x_k^{(j)}|$ is the distance between the kth components of sample points $\boldsymbol{x}^{(i)}$ and $\boldsymbol{x}^{(j)}$. After building a high-precision surrogate model, tunnel engineering data can be used to build an accurate TBM thrust model. The KRG model of thrust of the TBM is trained with 200 sample points to determine the unknown parameters of the relationship. To sum up, after the screening of the main factors, the accuracy of the surrogate model has been effectively improved, and the KRG model will be used to predict the thrust force of TBM in the future.

4 Thrust force prediction with the KRG model

4.1 Evaluation standard on the thrust prediction

According to the established thrust model (KRG model) for predicting the thrust force, the standard for evaluating the prediction result is measured by relative error. The equation of the relative error ε_{a} is shown as:

$$\varepsilon_{\mathrm{a}}=\frac{\left|F_{\mathrm{c}}-F_{\mathrm{p}}\right|}{F_{\mathrm{c}}}\times 100\%, \tag{18}$$

where F_{c} and F_{p} represent actual test values and predicted test values, respectively.

4.2 Comparison of prediction results in different modeling sections

To make the thrust prediction model of TBM applicable in the actual situation, the thrust models of different excavation positions are established in this study. The thrust models A–C of three different excavation positions are established respectively and are set up in the database. The same KRG model is used to predict the thrust of the above three thrust models of TBM in the unexcavated section. To compare the prediction accuracy of the three models, different models are used for prediction and comparison in the

same excavated area. The flow chart of the above prediction method is shown in Fig. 5.

Based on the above methods, three KRG thrust models are used to predict the unexcavated part and compared with the recorded site data. In addition, the statistical analysis of the relative error is used to measure the accuracy of the prediction of the unconsolidated section. The analysis of three thrust prediction models based on different excavation positions is as follows.

4.2.1 KRG model A

As shown in Fig. 6, the KRG model A is built in the excavated section A to predict the unexcavated sections A1, A2, and A3. Based on the excavated sample data, prediction model A is established using the KRG model.

The ranges of the three prediction samples are A_1=[1121.61, 1122.00] m, A_2=[1124.25, 1124.50] m, A_3=[1127.80, 1128.40] m. The predicted value based on the surrogate model is compared with the actual engineering data recorded on site. As shown in Fig. 7, the thrust prediction value of KRG model A is basically consistent with the actual value of the unconsolidated section A1, while there is a large deviation between the thrust prediction value and the actual value in the A2 and A3 sections.

As shown in Fig. 8, with the increase of prediction distance, the relative error of the three different

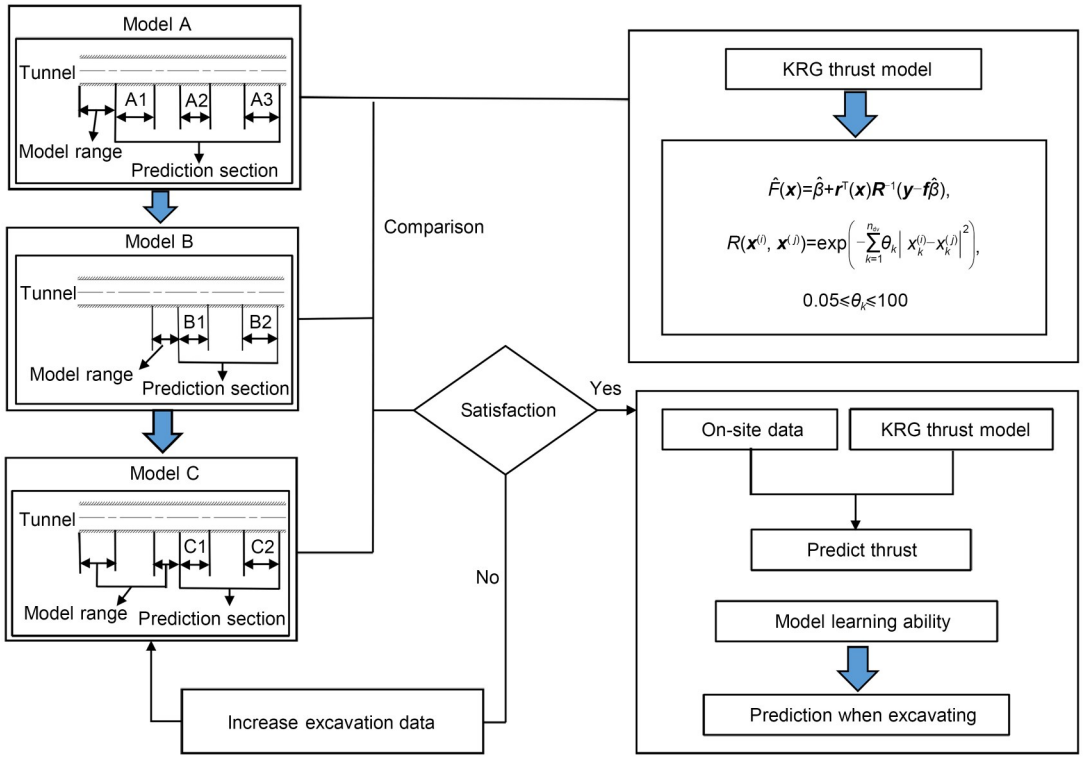

Fig. 5 Flow chart of thrust prediction comparison

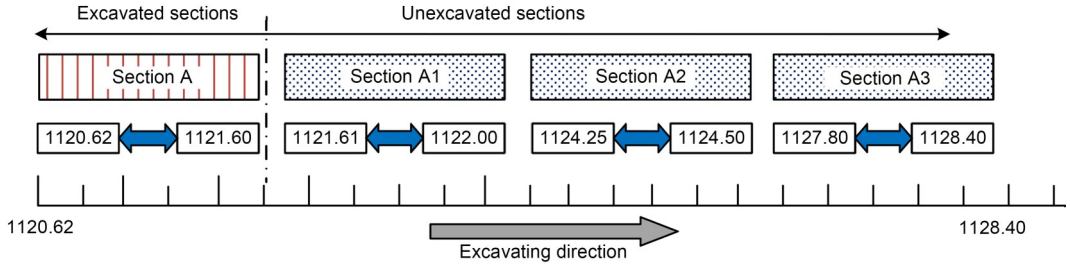

Fig. 6 Distribution map of sample data (unit: m)

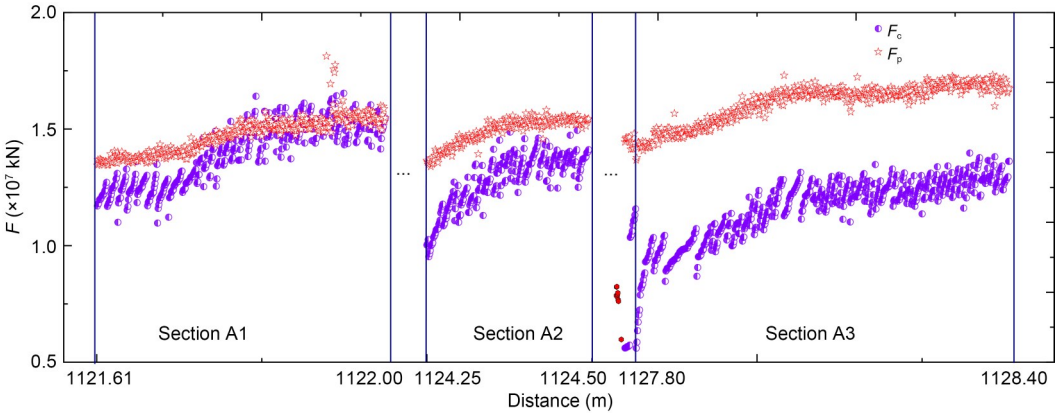

Fig. 7 Thrust prediction of unexcavated sections A1, A2, and A3 by model A

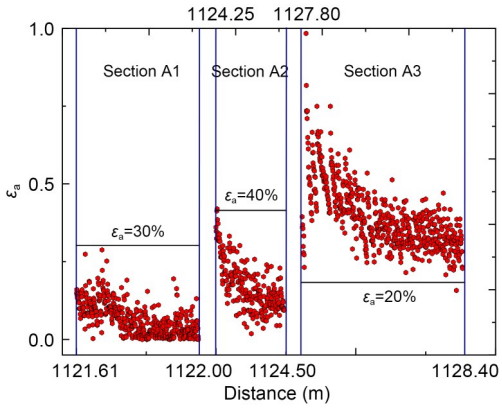

Fig. 8 Relative error of the thrust force prediction by model A

distance prediction values gradually increases. The relative error value of the unexcavated part A1 is less than 30%, and the relative error value of A2 is less than 40%, but the error value of A3 is generally greater than 20%. Compared A3 with A1 and A2, the ε_a value is increasing, which shows that the predicted value of thrust force gradually deviates from the actual value as the predicted distance increases. There are two possible reasons why the thrust prediction model based on model A has the problem that the accuracy decreases with the increase of distance. One possible reason is that when the part not mined is closer to the modeling sample data part, the prediction accuracy is higher, but the farther away from the modeling sample data part, the lower the prediction accuracy. Another is that the KRG model is not suitable for prediction. To prove this possibility, KRG model B is established. The sample data are from the previous sections of unexcavated section A2. Model B is applied to predict sections B1 and B2.

4.2.2 KRG model B

KRG model B is built in the excavated section B to predict the unexcavated sections B1 and B2. To verify whether the reduction of thrust prediction accuracy is caused by the increase of distance, the excavated road sections different from model A are selected in the modeling process of model B. As shown in Fig. 9, the range of thrust model modeling section B is $B=[1123.44, 1124.24]$ m. The ranges of thrust model prediction sections B1 and B2 based on the surrogate model are $B_1=[1124.25, 1124.50]$ m and $B_2=[1127.80, 1128.40]$ m. As shown in Fig. 10, for model B, comparing the unexcavated sections B1 and B2, the prediction of thrust forces is closer to the actual value in section B1. In addition, comparing the relative error values of B1 and B2, the relative error of unexcavated section B2 (ε_a>30%) is obviously higher than that of unexcavated section B1 (ε_a<25%). As shown in Fig. 11, the prediction result is basically consistent with that of model A. With the increase of the prediction distance, the relative error between the predicted value of the surrogate model and the actual value gradually increases, which also verifies the first possible reason. However, the above two models do not verify the thrust prediction ability of the KRG model. Therefore, a third model is established, based on the above two models, to verify the second possibility.

4.2.3 KRG model C

KRG model C is built in the excavated section B and section A to predict unexcavated sections C1 and C2. As shown in Fig. 12, the sample data of model C are from excavated section C, including section A and

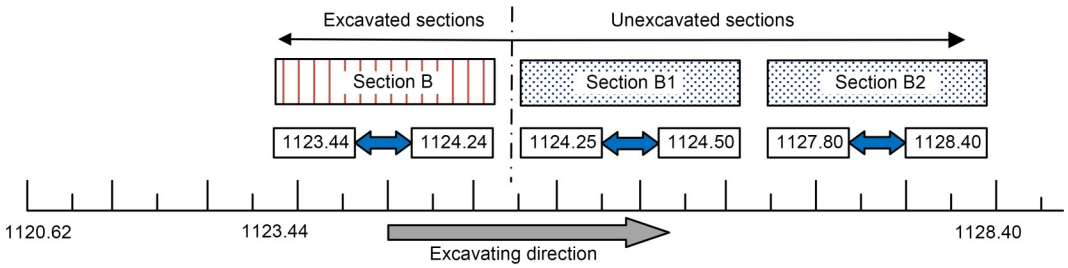

Fig. 9 Distribution diagram of sample data (unit: m)

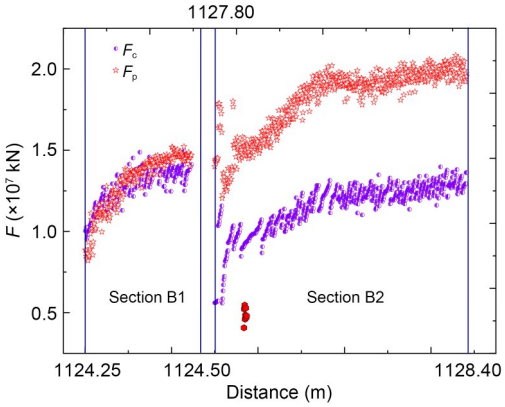

Fig. 10 Thrust prediction of unexcavated sections B1 and B2 by model B

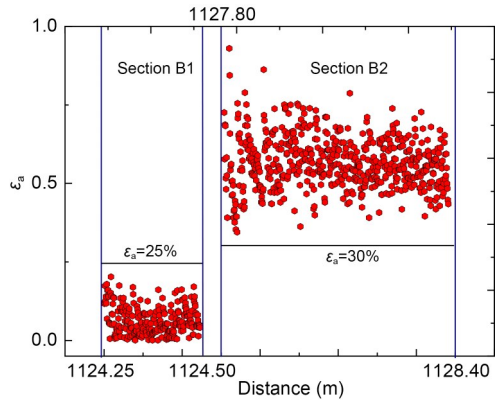

Fig. 11 Relative error of the thrust force prediction by model B

section B. The predicted ranges of sections C1 and C2 based on the KRG model are C_1=[1124.25, 1124.50] m and C_2=[1127.80, 1128.40] m. As shown in Fig. 13, compared with models A and B, the thrust prediction model based on model C has better prediction results. The prediction results show that the thrust prediction results of model C are basically consistent with the field engineering data. On this basis, the relative error between the thrust prediction model of the TBM based on the KRG model and the actual value is less than 30%. As shown in Fig. 14, the accuracy of thrust prediction results will not decrease with the increase of prediction distance, indicating that the TBM thrust prediction model based on model C has a high accuracy. In addition, the high accuracy of model C also shows that the KRG model can be used to predict the thrust of the TBM.

Compared with models A and B, the higher prediction accuracy of model C shows that when the thrust modeling and predicted working conditions are similar, the predicted uncut section is the same, and the predicted thrust value of the TBM based on the proxy model is basically the same as the actual value. Meanwhile, it can be seen that model C has continuous learning ability and predictive ability with increasing excavated distance. As a matter of fact, the sample data of model C consist of two parts, section A and section B. Comparing the predicted values and real values of the thrust force, it is confirmed that model C has a better prediction. Therefore, the thrust model based on surrogate model provides a high precision method for better thrust prediction of a TBM.

The results and analysis above demonstrate that the proposed approach can not only accurately predict the dynamic thrust force of the load but can also precisely estimate its statistical characteristics, which is of great help for the design and analysis of TBMs. In addition, numerous post-hoc analyses can be performed based on the prediction model. For instance, researchers can use global sensitivity analysis to understand how the operation parameters interact with each other or to locate the key operation parameters under different working conditions. Besides, the performance prediction results can improve excavation planning. For example, researchers can maximize the advance rate based on the performance prediction model in this paper. In addition, the proposed approach

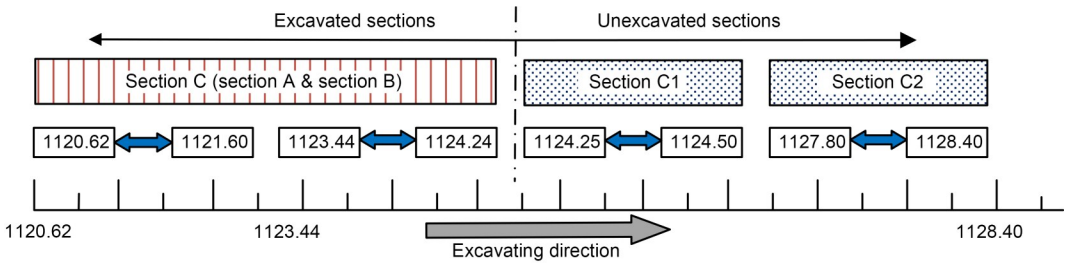

Fig. 12 Distribution diagram of sample data (unit: m)

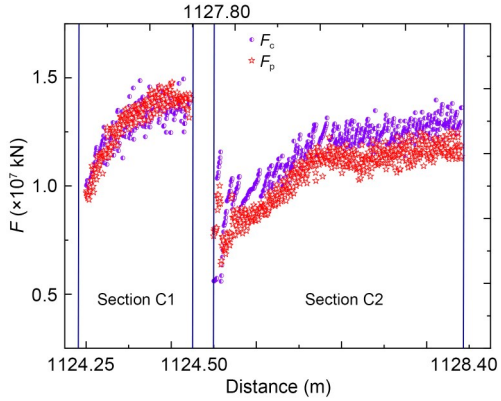

Fig. 13 Thrust prediction in unexcavated sections C1 and C2 by model C

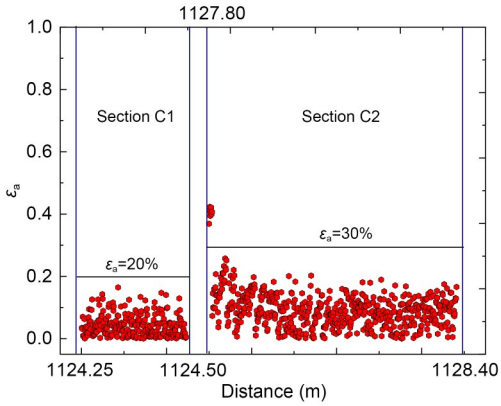

Fig. 14 Relative error of the thrust force prediction by model C

can construct a prediction model based on different engineering data (Sun et al., 2018).

5 Discussion

In addition, when the above three models are predicted in farther sections, the predicted value of TBM thrust is not the same as the real value. In model A and model B, the thrust prediction value will be greater than the actual value in most cases. Compared with models A and B, the prediction error of model C is effectively reduced. However, when model C predicts the thrust in the farther section, we find that the predicted thrust is often smaller than the actual value. On the one hand, because the process of TBM thrust prediction is inherently random, the problem that the predicted value is different from the actual value occurs. The thrust is not only affected by the factors of the shield machine itself (e.g. the tunneling speed, the rock pressure of the shield machine, and the water pressure of the cutterhead), but also by the geological conditions and the rock stripping process. In addition, the sensor will also be disturbed by noise in the process of recording data, which will cause some errors in the monitoring of the true value of thrust. On the other hand, the generalization ability of the KRG model is limited. With the increase of prediction distance, the continuous addition of noise factors will have a certain impact on the overall performance of the prediction model. That is, there will be a certain deviation between the predicted value and the actual value of the thrust, and the predicted value will be smaller or larger than the actual value.

In the process of factor screening using the Morris method, it can be found that the tunneling speed is the most important factor affecting the mean value of thrust prediction. In the process of thrust modeling, the change of tunneling speed often leads to a difference between the predicted value and the actual value of TBM thrust. Therefore, in the process of practical application, when there is a big gap between the predicted value and the actual value monitored by the sensor, the TBM parameters such as tunneling speed should be adjusted in time.

Compared with the limited generalization ability of the KRG model, various neural network models incorporate uncertainty and previous information into data-driven models, which can significantly improve

the generalization ability of prediction models (Zhang et al., 2022b). Therefore, future research work will focus on improving the generalization ability of the TBM thrust prediction model. In addition, software development and user guide interface can significantly improve the applicability of the data-driven model, thus enhancing the application of TBM thrust prediction model in engineering practice (Zhang et al., 2022a).

6 Conclusions

In this paper, a new method of modeling and predicting thrust force for the mass on-site data is proposed, which integrates operation parameter analysis and thrust prediction analysis. Based on the work in this study, the following conclusions can be drawn.

To establish the thrust prediction model of the TBM, the composition and influencing factors of TBM thrust are analyzed. To overcome the difficulty of thrust modeling of the TBM, a surrogate model is used to train engineering sample data to obtain the corresponding relationship between thrust and its influencing factors. After using the Morris method to screen the main factors, the accuracy of the surrogate model is greatly improved. The TBM thrust prediction model based on the KRG model shows that the error between the predicted thrust value and the actual value is small when the number of training samples is increased and the working conditions of thrust modeling and prediction are the same. Therefore, thrust modeling based on a data-driven surrogate model can be used as the theoretical basis for thrust determination in TBM forward excavation construction control. It may also offer new research concepts for mass measured data analysis and modeling of complex engineering equipment characterized by nonlinearity and multiple influencing factors.

Acknowledgments

This work is supported by the National Natural Science Foundation of China (No. 5217052098) and the National Key Research and Development Program of China (No. 2020YFB2007203).

Author contributions

Lintao WANG conducted the modeling and theoretical derivation of the approximate model and trained the sample of the approximate model. Jie LI analyzed the thrust composition and influencing factors of TBM and modeled the thrust of TBM by using agent model technology based on field data. Fengzhang ZHU improved the accuracy of the surrogate model greatly after the principal factor screening based on the Morris method, and wrote the first draft of the paper. Wei SUN revised and edited the final version.

Conflict of interest

Lintao WANG, Fengzhang ZHU, Jie LI, and Wei SUN declare that they have no conflict of interest.

References

Barton NR, 1999. TBM performance estimation in rock using Q(TBM). *Tunnels & Tunnelling International*, 31(9):30-34.

Breiman L, 2001. Random forests. *Machine Learning*, 45(1): 5-32. https://doi.org/10.1023/A:1010933404324

Buhmann MD, 2000. Radial basis functions. *Acta Numerica*, 9:1-38. https://doi.org/10.1017/S0962492900000015

Copur H, Aydin H, Bilgin N, et al., 2014. Predicting performance of EPB TBMs by using a stochastic model implemented into a deterministic model. *Tunnelling and Underground Space Technology*, 42:1-14. https://doi.org/10.1016/j.tust.2014.01.006

Gutmann HM, 2001. A radial basis function method for global optimization. *Journal of Global Optimization*, 19:201-227. https://doi.org/10.1023/A:1011255519438

Hassanpour J, Rostami J, Khamehchiyan M, et al., 2010. TBM performance analysis in pyroclastic rocks: a case history of Karaj water conveyance tunnel. *Rock Mechanics and Rock Engineering*, 43(4):427-445. https://doi.org/10.1007/s00603-009-0060-2

Huo JZ, Zhang HD, Xu ZH, et al., 2022. Coupling dynamic characteristics of tunnel boring machine cutterhead system with multi-source uncertainties. *Engineering Failure Analysis*, 137:106180. https://doi.org/10.1016/j.engfailanal.2022.106180

Iliadis L, Jayne C, Tefas A, et al., 2022. Engineering Applications of Neural Networks. Springer, Cham, Germany. https://doi.org/10.1007/978-3-031-08223-8

Jean WH, Sutikno P, Fan SZ, et al., 2022. Comparison of deep learning algorithms in predicting expert assessments of pain scores during surgical operations using analgesia nociception index. *Sensors*, 22(15):5496. https://doi.org/10.3390/s22155496

Krause H, 1976. Geologische erfahrungen beim einsatz von tunnelvortriebsmaschinen in Baden-Württemberg. *In*: für Geomechanik ÖG (Ed.), Neue Erkenntnisse im Hohlraumbau—Fundierungen im Fels/Latest Findings in the Construction of Underground Excavations—Rock Foundations. Springer, Vienna, Austria, p.49-60 (in German).

https://doi.org/10.1007/978-3-7091-8452-3_3

Li WJ, Zeng QL, Yin L, et al., 2011. Analysis on force model of wedge-shaped milling cutters and influence laws. *Mining & Processing Equipment*, 39(10):112-117 (in Chinese). https://doi.org/10.16816/j.cnki.ksjx.2011.10.029

Lin SS, Zhang N, Zhou AN, et al., 2022. Time-series prediction of shield movement performance during tunneling based on hybrid model. *Tunnelling and Underground Space Technology*, 119:104245. https://doi.org/10.1016/j.tust.2021.104245

Lv F, Yu J, Zhang J, et al., 2022. A novel stacking-based ensemble learning model for drilling efficiency prediction in earth-rock excavation. *Journal of Zhejiang University-SCIENCE A (Applied Physics & Engineering)*, 23(12): 1027-1046. https://doi.org/10.1631/jzus.A2200297

Masi F, Stefanou I, Vannucci P, et al., 2021. Thermodynamics-based artificial neural networks for constitutive modeling. *Journal of the Mechanics and Physics of Solids*, 147: 104277. https://doi.org/10.1016/j.jmps.2020.104277

Meng XH, Babaee H, Karniadakis GE, 2021. Multi-fidelity Bayesian neural networks: algorithms and applications. *Journal of Computational Physics*, 438:110361. https://doi.org/10.1016/j.jcp.2021.110361

Morris MD, 1991. Factorial sampling plans for preliminary computational experiments. *Technometrics*, 33(2):161-174. https://doi.org/10.2307/1269043

Mullur AA, Messac A, 2006. Metamodeling using extended radial basis functions: a comparative approach. *Engineering with Computers*, 21(3):203-217. https://doi.org/10.1007/s00366-005-0005-7

Myers RH, Montgomery DC, Anderson-Cook CM, 2016. Response Surface Methodology: Process and Product Optimization Using Designed Experiments. 4th Edition. John Wiley & Sons, Hoboken, USA.

Raissi M, Perdikaris P, Karniadakis GE, 2019. Physics-informed neural networks: a deep learning framework for solving forward and inverse problems involving nonlinear partial differential equations. *Journal of Computational Physics*, 378:686-707. https://doi.org/10.1016/j.jcp.2018.10.045

Regis RG, Shoemaker CA, 2005. Constrained global optimization of expensive black box functions using radial basis functions. *Journal of Global Optimization*, 31(1):153-171. https://doi.org/10.1007/s10898-004-0570-0

Rosso MM, Marasco G, Aiello S, et al., 2023. Convolutional networks and transformers for intelligent road tunnel investigations. *Computers & Structures*, 275:106918. https://doi.org/10.1016/j.compstruc.2022.106918

Sacks J, Welch WJ, Mitchell TJ, et al., 1989. Design and analysis of computer experiments. *Statistical Science*, 4(4): 409-423. https://doi.org/10.1214/ss/1177012413

Saltelli A, Tarantola S, Campolongo F, et al., 2004. Sensitivity Analysis in Practice: a Guide to Assessing Scientific Models. Wiley, Hoboken, USA.

Shi H, Yang HY, Gong GF, et al., 2011. Determination of the cutterhead torque for EPB shield tunneling machine. *Automation in Construction*, 20(8):1087-1095. https://doi.org/10.1016/j.autcon.2011.04.010

Sun W, Shi ML, Zhang C, et al., 2018. Dynamic load prediction of tunnel boring machine (TBM) based on heterogeneous in-situ data. *Automation in Construction*, 92:23-34. https://doi.org/10.1016/j.autcon.2018.03.030

Sun W, Peng X, Dou J, et al., 2020. Surrogate-based weight reduction optimization of forearm of bucket-wheel stacker reclaimer. *Structural and Multidisciplinary Optimization*, 61(3):1287-1301. https://doi.org/10.1007/s00158-019-02415-3

Tao Z, Tan XD, Han T, et al., 2010. Reconstruction of normal speech from whispered speech based on RBF neural network. Proceedings of the 3rd International Symposium on Intelligent Information Technology and Security Informatics, p.374-377. https://doi.org/10.1109/IITSI.2010.118

Williamson RC, Smola AJ, Scholkopf B, 2001. Generalization performance of regularization networks and support vector machines via entropy numbers of compact operators. *IEEE Transactions on Information Theory*, 47(6): 2516-2532. https://doi.org/10.1109/18.945262

Yagiz S, 2017. New equations for predicting the field penetration index of tunnel boring machines in fractured rock mass. *Arabian Journal of Geosciences*, 10(2):33. https://doi.org/10.1007/s12517-016-2811-1

Yang L, Meng XH, Karniadakis GE, 2021. B-PINNs: Bayesian physics-informed neural networks for forward and inverse PDE problems with noisy data. *Journal of Computational Physics*, 425:109913. https://doi.org/10.1016/j.jcp.2020.109913

Yuan XF, Wang YN, Sun W, et al., 2010. RBF networks-based adaptive inverse model control system for electronic throttle. *IEEE Transactions on Control Systems Technology*, 18(3):750-756. https://doi.org/10.1109/TCST.2009.2026397

Zhang P, Yin ZY, Jin YF, 2022a. Machine learning-based modelling of soil properties for geotechnical design: review, tool development and comparison. *Archives of Computational Methods in Engineering*, 29(2):1229-1245. https://doi.org/10.1007/s11831-021-09615-5

Zhang P, Yin ZY, Jin YF, et al., 2022b. Physics-informed multifidelity residual neural networks for hydromechanical modeling of granular soils and foundation considering internal erosion. *Journal of Engineering Mechanics*, 148(4): 04022015. https://doi.org/10.1061/(ASCE)EM.1943-7889.0002094

Zhang Q, Huang T, Huang GY, et al., 2013. Theoretical model

for loads prediction on shield tunneling machine with consideration of soil-rock interbedded ground. *Science China Technological Sciences*, 56(9):2259-2267. https://doi.org/10.1007/s11431-013-5302-6

Zhang Q, Qu CY, Cai ZX, et al., 2014. Modeling of the thrust and torque acting on shield machines during tunneling. *Automation in Construction*, 40:60-67. https://doi.org/10.1016/j.autcon.2013.12.008

Zhang ZH, Meng L, Sun F, 2014. Wear analysis of disc cutters of full face rock tunnel boring machine. *Chinese Journal of Mechanical Engineering*, 27(6):1294-1300. https://doi.org/10.3901/CJME.2014.0905.145

Zheng YL, Zhang QB, Zhao J, 2016. Challenges and opportunities of using tunnel boring machines in mining. *Tunnelling and Underground Space Technology*, 57:287-299. https://doi.org/10.1016/j.tust.2016.01.023